

2



Lawrence Berkeley Laboratory

UNIVERSITY OF CALIFORNIA

Materials & Chemical Sciences Division

Presented at the ASTM International Symposium on Fatigue Crack Closure, Charleston, SC, May 1986, and to be published in **Mechanics of Fatigue Crack Closure**, J.C. Newman, Jr. and W. Elber, Eds., American Society for Testing and Materials, Philadelphia, PA, 1988

RECEIVED
LAWRENCE
BERKELEY LABORATORY

MAY 10 1988

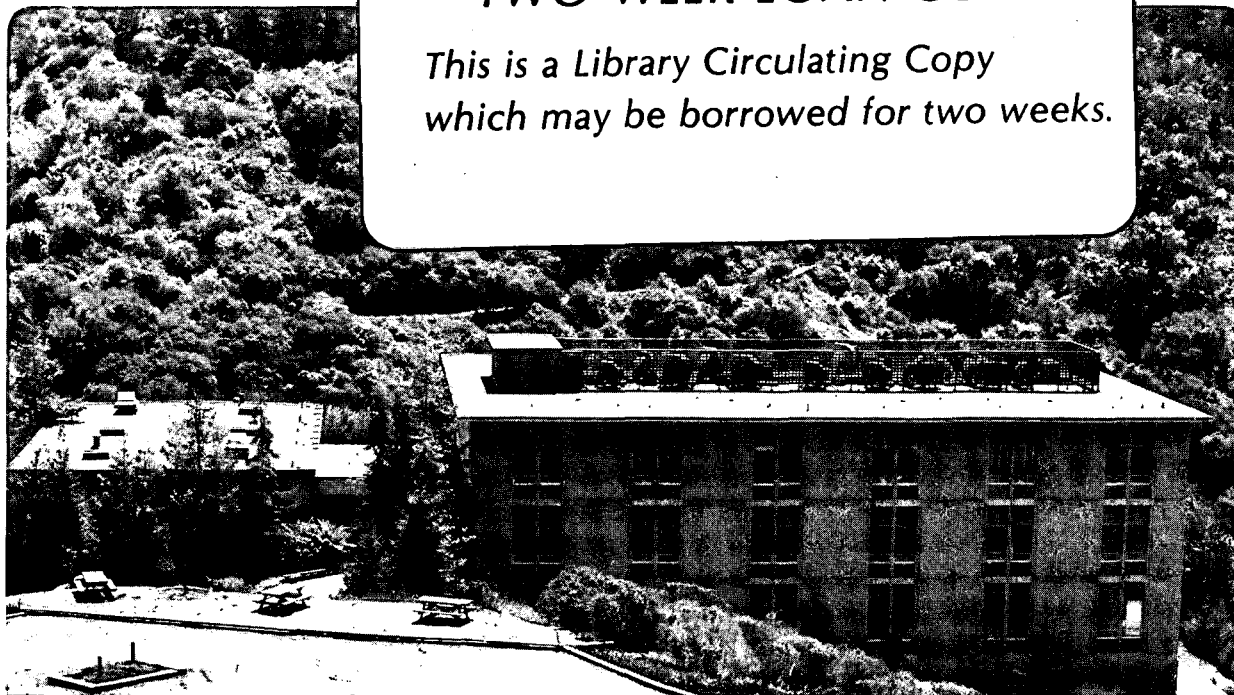
LIBRARY AND
DOCUMENTS SECTION

On the Role of Crack Closure Mechanisms in Influencing Fatigue Crack Growth Following Tensile Overloads in a Titanium Alloy: Near Threshold Versus Higher ΔK Behavior

C.M. Ward-Close and R.O. Ritchie

April 1986

TWO-WEEK LOAN COPY
This is a Library Circulating Copy which may be borrowed for two weeks.



LBL-21485

2

DISCLAIMER

This document was prepared as an account of work sponsored by the United States Government. While this document is believed to contain correct information, neither the United States Government nor any agency thereof, nor the Regents of the University of California, nor any of their employees, makes any warranty, express or implied, or assumes any legal responsibility for the accuracy, completeness, or usefulness of any information, apparatus, product, or process disclosed, or represents that its use would not infringe privately owned rights. Reference herein to any specific commercial product, process, or service by its trade name, trademark, manufacturer, or otherwise, does not necessarily constitute or imply its endorsement, recommendation, or favoring by the United States Government or any agency thereof, or the Regents of the University of California. The views and opinions of authors expressed herein do not necessarily state or reflect those of the United States Government or any agency thereof or the Regents of the University of California.

**ON THE ROLE OF CRACK CLOSURE MECHANISMS IN INFLUENCING FATIGUE
CRACK GROWTH FOLLOWING TENSILE OVERLOADS IN A TITANIUM ALLOY:
NEAR-THRESHOLD vs. HIGHER ΔK BEHAVIOR**

by

C. M. Ward-Close* and R. O. Ritchie

Materials and Molecular Research Division,
Lawrence Berkeley Laboratory
and

Department of Materials Science and Mineral Engineering,
University of California, Berkeley, CA 94720, U.S.A.

*Royal Aircraft Establishment, Farnborough, Hants, U.K.

April 1986

Presented at the ASTM International Symposium on
"Fatigue Crack Closure", Charleston, South Carolina, May 1986

This work was supported by the Director, Office of Energy Research,
Office of Basic Energy Sciences, Materials Sciences Division of the
U.S. Department of Energy under Contract No. DE-AC03-76SF00098.

**ON THE ROLE OF CRACK CLOSURE MECHANISMS IN INFLUENCING FATIGUE
CRACK GROWTH FOLLOWING TENSILE OVERLOADS IN A TITANIUM ALLOY:
NEAR-THRESHOLD vs. HIGHER ΔK BEHAVIOR**

C. M. Ward-Close¹ and R. O. Ritchie¹

REFERENCE: Ward-Close, C. M., and Ritchie, R. O., "On the Role of Crack Closure Mechanisms in Influencing Fatigue Crack Growth Following Tensile Overloads in Titanium Alloys," Fatigue Crack Closure, ASTM STP, J. C. Newman and W. Elber, Eds., American Society for Testing and Materials, Philadelphia, PA, 1987.

ABSTRACT: A comparative study has been made of the transient fatigue crack growth rate behavior following tensile overloads at low (near-threshold) and high stress intensity ranges in an α/β -type titanium alloy IMI 550, with specific emphasis of the role of crack closure mechanisms. After tensile overloads, fatigue cracks in both coarse-grained β -annealed and fine-grained α/β microstructures were observed initially to accelerate, followed by significant retardation, before growth rates returned to their baseline levels. The initial acceleration was attributed to an immediate reduction in near-tip closure, as indicated by metallographic sectioning, and a slight

¹Visiting Scientist and Professor, Materials and Molecular Research Division, Lawrence Berkeley Laboratory, and Department of Materials Science and Mineral Engineering, University of California, Berkeley, Calif 94720, U.S.A. Dr. Ward-Close is currently at the Royal Aircraft Establishment, Farnborough, Hants, U.K.

decrease in **far-field** closure, as measured by back-face compliance methods. Subsequent retardation was **not** associated with marked changes in far-field closure, although there were indications on compliance curves of a second "closure point" at a higher load, suggesting an approximate 50% increase in near-tip closure. Load interaction effects were found to be most severe where specific mechanisms of crack closure were prominent. Thus, the maximum post-overload retardations were seen in the coarse-grained α microstructure, and when baseline stress intensity ranges were close to the threshold ΔK_{TH} , or when the maximum overload stress intensities approached the fracture toughness.

KEY WORDS: fatigue (materials), crack (fracturing), crack propagation, variable amplitude loading, tensile overloads, crack closure, fatigue thresholds, titanium alloys.

Introduction

Transient fatigue crack growth rate behavior following load excursions from constant amplitude cycling have been reported in many investigations of fatigue life over the past two decades. Although such effects are clearly important in determining the fatigue endurance of many service structures and components, precise mechanistic origins remain unclear.

The most documented load interaction effect is that of crack growth rate retardation following a single tensile overload. Various mechanisms have been proposed to account for the post-overload retardation behavior, as illustrated schematically in Fig. 1. These mechanisms are based on concepts of a) residual stresses (1), where the higher strain generated by the overload results in an increase in the residual compressive stress field ahead of the crack on unloading; b) crack closure (2,3), where the residual stresses lead to enhanced plasticity-induced closure in the wake of the advancing crack; c) plastic blunting (4,5) of the crack tip at the overload; d) crack deflection (6), where the local "crack driving force" is reduced due to a deviation of the crack path following the overload; e) strain hardening (7,8), from either monotonic hardening of material in the overload plastic zone following tensile overloads or cyclic hardening after block loading sequences; and f) crack front profile (9), where, for high tensile overloads in thinner sheet, "pop-in" type crack extension at the overload precedes slower crack growth at the (plane stress) edges of the specimen.

Of these mechanisms, the role of the residual compressive stress field and the consequent effect of crack closure appear to provide a primary basis for rationalizing many of the observed effects. Accordingly, several successful models for the prediction of fatigue crack growth rates under variable amplitude/spectrum loading have been based on residual stress and closure concepts (e.g., refs. 10-12). The majority of supporting evidence on the specific role of crack closure, however, has been gathered at intermediate to high stress intensity ranges (2,3,6,12-15). Only limited work has been performed on variable amplitude loading at low stress intensities (16,17) approaching the fatigue threshold, ΔK_{TH} , below which cracks are presumed dormant. In fact, there have been few experimental studies which provide sound quantitative evidence for the effect of closure on transient crack growth behavior at **near-threshold levels**, i.e., under predominantly plane strain conditions (16,17). Von Euw et al. (3) report the existence of highly abraded post overload regions on fracture surfaces of a 2024-T3 aluminum alloy, which are an obvious indication of closure. Measurements of the change in closure, however, are conflicting. Davidson et al. (17) observed an increase in closure load using surface measurements on a powder aluminum alloy subject to large overloads. De Castro and Parks (16), conversely, report a decrease in closure load at the overload, using back-face strain compliance method on a low alloy steel.

The objective of the present study is to evaluate the load interaction effects following tensile overloads at both high and

near-threshold ΔK levels in a commercial α/β -type titanium alloy, heat treated to give different degrees of crack path deflection and roughness-induced crack closure (18-20). Specifically, the intent is to identify the role of crack closure through metallographic and compliance measurements of the quantitative changes in the closure stress intensity before and after the event.

Experimental Procedures

The material used in this investigation was a commercial α/β -type titanium alloy Ti-4Al-4Mo-2Sn-0.5Si (IMI 550), supplied in the form of 25 mm rolled plate. The alloy, which has been fully characterized in previous studies (21) with respect to variable amplitude fatigue behavior under simulated flight spectrum loading, was examined in two widely different microstructures (Fig. 2). These were i) a normal α/β -solution treated and aged condition (900°C, air cooled, 24 hr at 550°C), with a fine-grained microstructure consisting of 55% primary α (grain size $\sim 14 \mu\text{m}$) and transformed β , and ii) a β -solution treated and aged condition (1010°C, air cooled, 24 hr at 550°C), with a coarse-grained microstructure of 100% transformed β , containing large colonies of Widmanstätten α and a small volume fraction of grain boundary α (prior β grain size $\sim 240 \mu\text{m}$). Ambient temperature mechanical properties for the transverse direction are listed in Table 1.

Table 1. Ambient Temperature Mechanical Properties of IMI 550

<u>Microstructure</u>	<u>E</u>	<u>0.2% Yield Stress (σ_y)</u>	<u>UTS</u>	<u>Elong.</u>	<u>Redn. Area</u>	<u>K_{Ic}</u>
	(GPa)	(MPa)	(MPa)	(%)	(%)	(MPa \sqrt{m})
α/β annealed	126	1024	1135	11	34	85.8
β annealed	121	888	1102	9	14	99.5

Fatigue tests were performed on 10 mm thick compact C(T) test pieces machined in the L-T orientation. Tests were conducted with a baseline load ratio ($R = K_{min}/K_{max}$) of 0.1 at frequencies between 4 and 50 Hz (sine wave). Crack lengths were continuously monitored using a D.C. electrical potential system which incorporated load shedding to maintain constant ΔK conditions. Single tensile overloads were applied at 0.01 Hz with baseline loading maintained at constant ΔK . Fig. 3 illustrates the various parameters associated with the overload experiments. All tests were performed under predominantly plane strain conditions, as the maximum overload plastic zone never exceeded 1/50 of the test piece thickness.

The delay in growth rates induced by the overloads was quantified using the method depicted in Fig. 4. A crack size (a_1) was chosen beyond the overload point where growth rates had returned to the baseline (steady state) value, and the number of cycles (N) required to grow the crack to this distance noted. The distance the crack would have grown in N cycles without an overload was calculated

(a_2), and the difference (a_D) was defined as the delay distance. The number of delay cycles equivalent to this distance were then calculated using the baseline crack growth rate $(da/dN)_B$. The use of a delay distance to quantify overload retardation was considered to be preferable to a simple cycles calculation, as it enables a direct comparison to be made between overloads applied at different baseline ΔK levels.

Crack closure was assessed globally using a back-face strain technique, where the closure stress intensity K_{C1} , at first contact of the crack surface, was determined from changes in slope of the elastic unloading curve. Based on such K_{C1} data, the local "crack driving force" was estimated in terms of an effective stress intensity range $\Delta K_{eff} = K_{max} - K_{C1}$. An offset elastic-displacement method was used to improve sensitivity, i.e., the displacement signal was offset by an amount proportional to the applied load such that the linear (crack open) portion of the compliance curve became constant with load (Fig. 5). The resultant load/displacement signal could then be amplified to exaggerate deviations from linearity caused by crack closure. Using this technique, two distinct indications of crack surface contact could be detected under certain circumstances, indicating changes in both near-tip and far-field closure.

Fractography was performed using both optical and scanning electron microscopy (SEM). In addition, crack path sections were

taken metallographically at the center of the specimen, impregnated with epoxy for edge retention, and imaged by optical microscopy.

Results

Constant Amplitude Cycling

Constant amplitude fatigue crack propagation rate data for IMI 550 are shown in Fig. 6, and indicate that the coarser-grained β -annealed microstructure shows lower growth rates than the α/β structure over the entire range of ΔK levels. Fractographically, fatigue surfaces in both structures appeared to be somewhat crystalline in nature, showing evidence of characteristic "cyclic cleavage" facets at low stress intensities, from failure of the α phase on or near the basal plane in the hexagonal crystal structure (Fig. 7). Fatigue cracks in the β -annealed structure, however, were far more irregular and tortuous, compared to the relatively flat and featureless crack surfaces in the finer-grained α/β structure (Fig. 8). This is particularly apparent in macroscopic views of the fracture surfaces shown in Fig. 9. Fatigue surfaces in the α/β structure can be seen to be quite smooth, and to highlight clearly the "beach marks" caused by the tensile overloads. By comparison, in the β -annealed structure, such markings are obscured by a fracture surface comprised primarily of coarse crystalline facets (Fig. 9).

Variable Amplitude Loading

Load interaction studies were initially confined to single overloads at 100 and 150% above the baseline K_{\max} , for two baseline ΔK levels of $8 \text{ MPa}\sqrt{\text{m}}$ and $15 \text{ MPa}\sqrt{\text{m}}$. These results are presented in Fig. 10. Each curve represents the best fit to data from up to six tests.

Growth Rate Data: At a baseline ΔK of $15 \text{ MPa}\sqrt{\text{m}}$, the initial effect of a 100% tensile overload was to induce a small increment of crack growth. Electrical potential measurements suggested crack advance over roughly $50 \mu\text{m}$, roughly consistent with metallographic sections through overloaded cracks in the α/β -annealed microstructure (Fig. 11). The overload clearly caused blunting of the crack, which resulted in an opening of the normally narrow crack over distances of some $100 \mu\text{m}$ behind the original (pre-overload) crack tip. In addition, the extension at the overload was highly irregular and showed clear evidence of roughness-induced closure from asperity contact at zero load (Fig. 11a), apparently from a mechanism of ductile tearing (Fig. 11b). No evidence of such crack extension at the overload was detected for corresponding tests at a baseline ΔK of $8 \text{ MPa}\sqrt{\text{m}}$.

Post-overload behavior was characterized by an initial acceleration (of ~ 1 to 2 orders of magnitude), followed by an abrupt deceleration (of ~ 1 order of magnitude below the baseline rate), and then a gradual return to steady state (Fig. 10a and 10b). At low

baseline ΔK levels ($8 \text{ MPa}\sqrt{\text{m}}$), crack growth retardation was far more severe in the coarse-grained β -annealed structure; the delay distance was over two times larger and the number of cycles of delay nearly 10 times larger than in the α/β -annealed structures (Fig. 10a). At higher baseline ΔK levels ($15 \text{ MPa}\sqrt{\text{m}}$), the effects were qualitatively similar, although the extent of crack growth affected by the overload was significantly larger and differences between the two microstructures were less apparent. In all cases, the distance, over which crack growth was retarded by the overloads, was well in excess of the computed maximum extent of the overload plastic zone size (Table 2).

Table 2. Data on Single Overload

<u>Microstructure</u>	<u>Baseline</u>	<u>100% Overload</u>	<u>100% Single Overload</u>	
	<u>ΔK</u> ($\text{MPa}\sqrt{\text{m}}$)	<u>Plastic Zone*</u> (mm)	<u>Delay Dist.</u> (mm)	<u>Delay Cycles</u>
α/β annealed	8	0.04	0.22	35,550
	15	0.14	0.88	9,370
β -annealed	8	0.05	0.52	301,190
	15	0.18	0.77	16,790

* computed from $1/2\pi (K_{OL}/\sigma_y)^2$

Fractography: A number of test pieces were metallographically polished prior to testing, and fatigue cracks were photographed at

various stages in the overload experiments. Other tests were halted at various stages, and sectioned to show internal crack profiles. Fig. 12 illustrates the behavior of a fatigue crack in α/β -annealed material subjected to a series of single and block overloads. The center section crack profile reveals metallographic evidence of crack closure (i.e., asperity contact) at zero load immediately following both a single overload, and a step down from a high block, and also in those sections of the crack formed during high block cycling. The role of deflection, however, is less clear. Stepping down after a 100% overload block to a ΔK of $15 \text{ MPa}\sqrt{\text{m}}$ caused crack deflection (of the order of 45°) at the surface in roughly half the tests, but not in the interior. Stepping down from a 150% overload block produced crack deflection at both the surface and interior (Fig. 12). Crack deflection, however, was rarely seen following 100 or 150% single tensile overload cycles.

Fatigue Crack Closure: Global measurements of fatigue crack closure (i.e., far field) were made using back-face strain compliance in the α/β -annealed microstructure, both before and after single tensile overloads at baseline ΔK levels of 8 and $15 \text{ MPa}\sqrt{\text{m}}$. In all cases, prior to the overload, the closure load was delineated by a single clear change in slope of the compliance curve during unloading (i.e., point C in Fig. 5). **No significant change in (far-field) closure load was found following single overloads at the lower baseline ΔK .** However, at a baseline ΔK of $15 \text{ MPa}\sqrt{\text{m}}$, a small

reduction in closure load was detected immediately after a 150% overload, implying an initial increase in ΔK_{eff} (Fig. 13). From five separate tests, the average decrease in closure load at the overload was 11%, with a range of 8 to 17%. Such reduced far-field closure over the length of the crack is consistent with the metallographic sections shown in Fig. 11a, which clearly indicate residual opening of the crack at zero load over some considerable distance behind the tip, due to gross blunting of the tip at the overload.

Despite the lack of radical changes in far-field crack closure following 100 and 150% overloads at $\Delta K = 15 \text{ MPa}\sqrt{\text{m}}$, there were definite indications on the back-face strain compliance traces of a second change in slope which began at the point of minimum (retarded) growth rates (i.e., point B in Fig. 5). This second slope change was smaller and occurred at a higher load in the fatigue cycle. Based on the evidence from metallographic sections of obvious crack face contact in the post-overload region (Figs. 11 and 12), it was reasoned that this slope change was associated with crack closure in this region just behind the crack tip, termed near-tip closure. In an attempt to verify this, a series of strain gauges were mounted on the side-face of a specimen of the α/β -annealed microstructure containing a 32 mm long crack. The gauges were mounted 5 mm above the crack plane and were spaced 5 mm apart along the crack length. Following a 150% tensile overload, compliance traces taken from the gauge spaced less than 2 mm from the crack tip indicated an

approximately 20% higher closure load than one spaced 12 mm from the tip.

In Fig. 13, the variation in measured closure loads with post-overload growth rate behavior is shown for 100 and 150% single overloads in the α/β -annealed microstructure. It can be seen that during the significant delayed retardation in growth rates following the overload (i.e., by three orders of magnitude for the 150% overload), the variation in near-tip closure, as defined by the ratio of effective to nominal ΔK , exactly tracks the changes in growth rates, whereas far-field closure is essentially unchanged. Such results are consistent with the early observations of Paris and Hermann (22) of variations in an "upper" and "lower" opening load following single tensile overloads.

Discussion

The results of this investigation clearly demonstrate that significant load interaction effects can take place under predominantly plane strain conditions, and that crack closure is an important mechanism in controlling load interaction response. However, unlike behavior at higher ΔK levels under predominantly plane stress conditions (23,24), the relevant mechanisms of crack closure are not simply associated with the plastic wake, i.e., plasticity-induced closure (2), and thus are not necessarily enhanced at the surface. Conversely, at low ΔK levels, the major mechanisms of closure appropriate to post-overload growth rates appear to result

from wedge shielding processes, in this alloy primarily from the contact of fracture surface asperities, i.e., roughness-induced closure (18-20), although this contact is clearly promoted by plastic strain in the wake of the crack. Modelling studies (25,26) of the closure generated by such wedging phenomena indicate that contact close to the tip has a far greater influence on the effective stress intensity range than contact remote from the tip. Since it is this near-tip closure which is primarily affected by the load excursions, the standard global measurement techniques, e.g., relying on test piece compliance, are likely to be relatively insensitive to the overload-induced changes. For this reason, it is important to distinguish near-tip closure (as measured in an SEM (17) or as in the present study) with that measured macroscopically from test piece compliance, as it is the local field which primarily dictates crack growth behavior.

Mechanisms: Far Field vs. Near-Tip Closure

As noted above, following a single tensile overload, it is the changes in near-tip crack closure which appear to control crack growth behavior. However, initially, the effect of the overload is to blunt the crack, which induces crack opening for a short distance behind the tip (Figs. 11 and 12). This removes the closure from where it has maximum influence on the effective ΔK , and would account for the initial acceleration of baseline crack growth rate following an overload. This is also supported by the observation that far-

field closure, measured by back-face strain, decreases on application of an overload (Fig. 13). The decrease in far-field closure is only of the order of 10%, which is not enough to account for the post-overload crack growth rate acceleration. However, the change in far-field closure is thought to be a secondary effect compared to the complete removal of near-tip closure (see also experimental observations in ref. 22).

The overload may, or may not, produce a significant increment of crack growth. However, those increments which were large enough to be measured, were found to be larger than would have been expected from the constant amplitude fatigue data. The exact reason for this is not known, but it may be a combination of several factors. The compressive residual stresses ahead of the baseline fatigue crack will be much lower than would normally be associated with a crack growing under continuous cycling at the overload level. Therefore the single overload cycle will generate more plastic deformation than it would if it were part of continuous cycling at that level, and hence produce a larger increment of growth. The fractographic evidence suggests that the overload growth increment will be highly ductile, and will produce non-matching fracture surfaces, which are subject to closure on return to baseline cycling. This closure may partly negate the acceleration effect of opening the crack tip and removing crack closure behind the pre-overload crack front. In support of this suggestion, the greatest post-overload accelerations were observed at the lowest baseline ΔK of $8 \text{ MPa}\sqrt{\text{m}}$.

It is generally agreed that, following an overload, residual strain produces residual stresses ahead of the crack, on unloading (1,2). These stresses will effectively reduce the load ratio of the advancing fatigue crack, and thus a reduction in crack growth rates would be anticipated. The effective reduction in load ratio would promote closure of the post-overload crack, and, as the length of the crack increases this closure would exert an increasing influence on the effective ΔK , and the fatigue crack growth rates would fall. This is in agreement with the experimental observation of delayed retardation, and also the fractographic evidence of post-overload crack closure. An approximately 50% increase in near-tip crack closure was detected at this stage, for both 100% and 150% overloads in the α/β -annealed material. The fact that no change in the near-tip closure was detected prior to this, merely reflects the limit of sensitivity of the strain measurement system to crack length changes of about 40 μm . This, therefore, was the minimum distance for detection of crack closure behind the crack front.

Based on observations in high strength aluminum alloys (27), it has recently been suggested that the retardation induced by the single overload results from significant crack branching, and the consequent reduction in local "driving force" from crack deflection and subsequent roughness-induced closure (6). Although such branching was seen occasionally after step-down from high-low block loading sequences (Fig. 12), in this particular high strength titanium alloy, crack deflection did not appear to be a dominant

mechanism in inducing the retardation. However, since post-overload growth rates approach near-threshold levels, the fracture mechanisms appropriate to this regime, namely crystallographic crack advance and enhanced roughness-induced crack closure, do act to further reduce ΔK_{eff} and hence to prolong the retardation (6). Accordingly, unlike load interaction effects at higher ΔK levels (3), under plane strain conditions the distance over which the crack is affected by the overload becomes far larger than the overload plastic zone (Table 2).

The overall retardation phenomenon due to a single tensile overload can thus be seen to result from a sequence of several mechanisms. At the overload, the crack blunts and is correspondingly opened for some distance behind the tip, leading to a **small reduction in far-field closure**. This, coupled with actual crack advance due to the overload, leads to an initial **increase** in growth rates. As the crack grows into the overload plastic zone, the increased residual compressive stresses promote crack surface contact (and consequent fracture surface abrasion) just behind the crack tip, leading to an **increase in near-tip closure** and hence to delayed retardation. In certain alloys, this process may be aided by crack deflection at the overload, which further reduces the local stress intensity (6). Finally, once retarded, the low ΔK_{eff} experienced by the crack induces such near-threshold mechanisms as local deflection, crystallographic growth and further closure from asperity contact, which prolong the retardation over distances beyond the extent of the overload plastic zone. However, as this zone passes further into the

crack wake, its effect diminishes with the result that growth rates progressively return to their baseline steady-state levels.

Microstructural Effects

In this study, it is apparent that the coarser-grained β -annealed microstructure showed the larger retardation effect following single tensile overloads (Fig. 10), consistent with prior simulated flight spectrum loading studies (21) where the fatigue lives of the α/β -annealed microstructures were 80% smaller. The effect, however, was more predominant at lower baseline ΔK levels. This is consistent with the far larger effective grain size of the β -annealed structure, which promotes crack deflection and crack path meandering (Fig. 8) and hence roughness-induced crack closure. In titanium alloys containing higher aluminum contents, where the propensity for planar slip is increased, this effect is likely to be enhanced further. At higher baseline ΔK levels, where wedge shielding mechanisms become less potent due to the larger crack opening displacements, the difference between the two microstructures is diminished. Presumably here, the slightly lower strength of the β -annealed structure favors plasticity-induced closure, but the effect is small.

The distinction between the effect of overloads at low (near-threshold) and high (near-instability) baseline ΔK levels can be seen in Fig. 14. Based on a further series of single 100% overloads, applied now to a range of baseline stress intensity ranges, it is

apparent that the magnitude of the retardation, whether measured in terms of delay distance or delay cycles, is increased either with decreasing ΔK towards the threshold or increasing ΔK towards instability. Similar observations have been reported for steels and aluminum alloys (14,15,28,29). However, unlike the results of Vecchio et al. (14) on aluminum alloys, the minimum delay was achieved at ΔK levels where the overload plastic zone was a much smaller fraction (0.01 to 0.02) of the test piece thickness. Such behavior reflects the contrasting mechanisms of crack growth retardation under plane stress and plane strain. In the one case, where behavior is dominated by plasticity-induced closure, with increasing ΔK , the tendency towards plane stress will promote this closure mechanism in the enlarged overload plastic zone. Thus, provided the zone does not become too large, such that the constraint of surrounding elastic material is lost, the load interaction effect will increase with increasing plastic zone size. Conversely, at low ΔK levels, where the crack opening displacements are small, the controlling mechanisms of closure are associated with wedging mechanisms. The potency of these mechanisms is enhanced where the size of the wedge is comparable with the crack opening displacements, such that plane strain load interaction effects tend to increase with decreasing ΔK level. Since the latter closure mechanisms are primarily microstructure-related, differences between the post-overload behavior of the α/β and β -annealed structures are likely to

be most apparent in this regime, consistent with the experimental results in Figs. 14 and 15.

Concluding Remarks

In this paper, we have attempted to highlight the close association between transient post-overload behavior of Mode I fatigue cracks and crack closure processes which rely on wedge mechanisms. This association can be further demonstrated by noting that Mode III (anti-plane shear) fatigue cracks, where crack closure via wedging is not relevant, show exactly the opposite behavior to Mode I cracks following such simple loading spectra (30,31). As illustrated in Table 3, the growth rates of Mode III cracks are increased after the application of a single positive overload,

Table 3. Transient Growth Rate Response of Mode I and Mode III Fatigue Cracks Following Simple Loading Spectra (30)

Load Sequence	Transient Growth Rate Response	
	Mode I	Mode III
	da/dN decreases	da/dN increases
	above effect reduced	above effect enhanced
	da/dN slower*	da/dN faster*

*Compared to steady-state da/dN at lower load level.

whereas Mode I growth rates are decreased. Similar differences occur for fully reversed overloads and block loading sequences. Although Mode III cracks do experience a form of closure, from the interference (i.e., friction, abrasion, etc.) between sliding crack surfaces, which similarly reduces the local "driving force" at the crack tip (31), it is not by a wedging mechanism. Correspondingly, the behavior of Mode III cracks following variable amplitude loading spectra is unimpeded by closure-related transient retardation/acceleration effects, and thus can be predicted simply from constant amplitude da/dN data (30).

Conclusions

Based on a study of single tensile overloads on fatigue crack propagation in titanium alloy IMI 550, heat treated to give coarse-grained transformed β and fine-grained α/β microstructures, the following conclusions can be made:

- 1) A single tensile overload was accompanied by crack tip blunting and a consequent immediate decrease in far-field crack closure, as measured globally using a back-face strain compliance technique. This resulted in an initial transient increase in crack growth rates.

- 2) Subsequent growth rates were found to experience significant delayed retardation, concurrent with an approximately 50% increase in post-overload near-tip crack closure, presumably due to the extension of the crack into the residual compressive stress field developed in

the overload plastic zone. Little evidence of crack branching/deflection could be detected in this alloy at the overload.

3) The magnitude of the load interaction effects was found to be larger in the coarse-grained β -annealed microstructure, particularly at near-threshold baseline ΔK levels, consistent with the greater propensity of this material for developing irregular crack paths and enhanced roughness-induced crack closure.

4) For a given microstructure, the magnitude of the load interaction effects was found to be promoted either with increasing ΔK or decreasing ΔK level, consistent with an increasing contribution from either closure induced by cyclic plasticity or closure induced by asperity wedging. Such behavior illustrates the essential difference between overload phenomena under plane stress and plane strain conditions.

Acknowledgements

This work was supported by the Director, Office of Energy Research, Office of Basic Energy Sciences, Materials Science Division of the U.S. Department of Energy under Contract No. DE-AC03-76SF00098, through the auspices of the Materials and Molecular Research Division of the Lawrence Berkeley Laboratory. Support for one of the authors (C.M.W-C.) was also provided by the Ministry of Defence, U.K., in the form of a leave of absence from the Royal Aircraft Establishment, U.K.

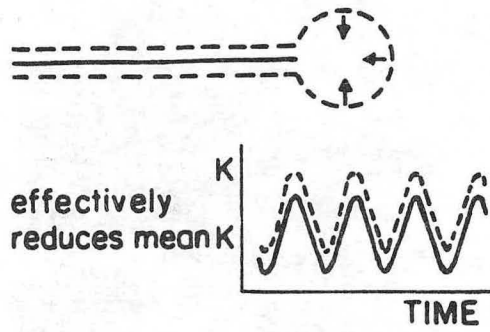
References

- (1) Schijve, J. "Fatigue Crack Propagation in Light Alloy Sheet Material and Structures," NRL Report MP 195, National Aeronautical and Astronautical Research Institute, Amsterdam, Holland, 1960.
- (2) Elber, W. in Damage Tolerance in Aircraft Structures, ASTM STP 486, American Society for Testing and Materials, Philadelphia, 1971, p. 230.
- (3) Von Euw, E. F. J., Hertzberg, R. W. and Roberts, R. in Stress Analysis and Growth of Cracks, ASTM STP 513, American Society for Testing and Materials, Philadelphia, 1973, p. 115.
- (4) Christensen, R. H. in Metal Fatigue, McGraw-Hill, New York, 1959.
- (5) Hudson, C. M. and Hardrath, H. F., "Effects of Changing Stress Amplitude on the Rate of Fatigue Crack Propagation of Two Aluminum Alloys," NASA Technical Note D-960, National Aeronautics and Space Administration, Washington, D.C., 1961.
- (6) Suresh, S., Engineering Fracture Mechanics, Vol. 18, 1983, p. 577.
- (7) Jones, R. E., Engineering Fracture Mechanics, Vol. 5, 1973, p. 585.
- (8) Knott, J. F. and Pickard, A. C., Metal Science, Vol. 11, 1977, p. 399.
- (9) Forsyth, P. J. E. in Fatigue 84, C. J. Beevers, ed., EMAS Ltd., Warley, U.K., Vol. 2, 1984, p. 637.

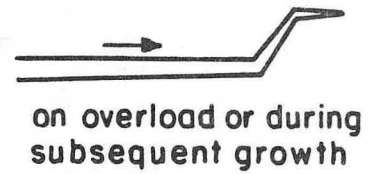
- (10) Dill, H. D. and Saff, C. R. in Fatigue Crack Growth Under Spectrum Loads, ASTM STP 595, American Society for Testing and Materials, 1976, p. 306.
- (11) Newman, J. C., Jr. in Methods and Models for Predicting Fatigue Crack Growth under Random Loading, ASTM STP 748, American Society for Testing and Materials, Philadelphia, 1981, p. 53.
- (12) de Koning, A. U. in Fracture Mechanics, 13th National Symposium, ASTM STP 743, American Society for Testing and Materials, Philadelphia, 1981, p. 63.
- (13) Musil, D. P. and Stephens, R. I. in Fracture 1977, D. M. R. Taplin, ed., University of Waterloo Press, Waterloo, Canada, Vol. 2, 1977, p. 1017.
- (14) Vecchio, R. S., Hertzberg, R. W. and Jaccard, R., Fatigue of Engineering Materials and Structures, Vol. 7, 1984, p. 181.
- (15) Vecchio, R. S., Hertzberg, R. W. and Jaccard, R., Scripta Metallurgica, Vol. 17, 1983, p. 343.
- (16) de Castro, J. T. P. and Parks, D. M., Scripta Metallurgica, Vol. 16, 1982, p. 1443.
- (17) Davidson, D. L., Hudak, S. J. and Dexter, R. J., "Measurement and Analysis of Critical Crack Tip Processes during Fatigue Crack Growth," NASA Contractor Report 172597, National Aeronautical and Space Administration, Langley Research Center, June 1985.
- (18) Walker, N. and Beevers, C. J., Fatigue of Engineering Materials and Structures, Vol. 1, 1979, p. 135.

- (19) Minakawa, K. and McEvily, A. J., Scripta Metallurgica, Vol. 15, 1981, p. 633.
- (20) Suresh, S. and Ritchie, R. O., Metallurgical Transactions A, Vol. 13A, 1982, p. 1627.
- (21) Ward-Close, C. M., International Journal of Fatigue, Vol. 6, 1984, p. 139.
- (22) Paris, P. C. and Hermann, L., in Fatigue Thresholds, J. Bäcklund, A. F. Blom, and C. J. Beevers, eds., EMAS Ltd., Warley, U.K., Vol. 1, 1982, p. 11.
- (23) Fleck, N. A. and Smith, R. A., International Journal of Fatigue, Vol. 4, 1982, p. 157.
- (24) Ray, S., Grandt, A. F. and Andrew, S. in Basic Questions in Fatigue, ASTM STP, J. T. Fong and R. J. Fields, eds., American Society for Testing and Materials, Philadelphia, PA, 1986.
- (25) Suresh, S. and Ritchie, R. O., Scripta Metallurgica, Vol. 17, 1983, p. 575.
- (26) Beevers, C. J. and Bell, K., Engineering Fracture Mechanics, Vol. 19, 1984, p. 93.
- (27) Lankford, J. and Davidson, D. L. in Advances in Fracture Research, D. Francois et al., eds., Pergamon Press, Oxford, U.K., Vol. 2, 1982, p. 899.
- (28) Ward-Close, C. M. and Ritchie, R. O., unpublished work, Lawrence Berkeley Laboratory, University of California, Berkeley, 1985.

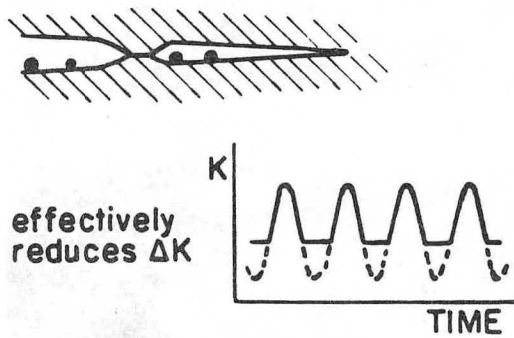
- (29) Chanani, G. R. in Flaw Growth and Fracture, ASTM STP 631, American Society for Testing and Materials, Philadelphia, PA, 1977, p. 365.
- (30) Nayeb-Hashemi, H., McClintock, F. A. and Ritchie, R. O., Engineering Fracture Mechanics, Vol. 18, 1983, p. 736.
- (31) Ritchie, R. O., McClintock, F. A. Tschegg, E. K. and Nayeb-Hashemi, H. in Multiaxial Fatigue, ASTM STP 853, K. J. Miller and M. W. Brown, eds., American Society for Testing and Materials, Philadelphia, PA, 1985, p. 203.



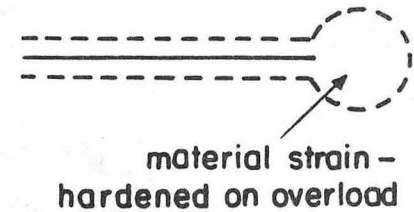
1) Residual Stress



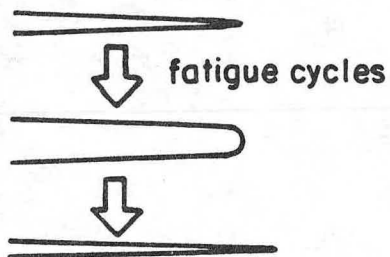
4) Deflection



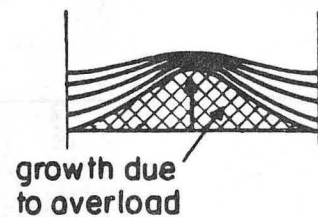
2) Crack Closure



5) Strain Hardening



3) Plastic Blunting/Re-sharpening

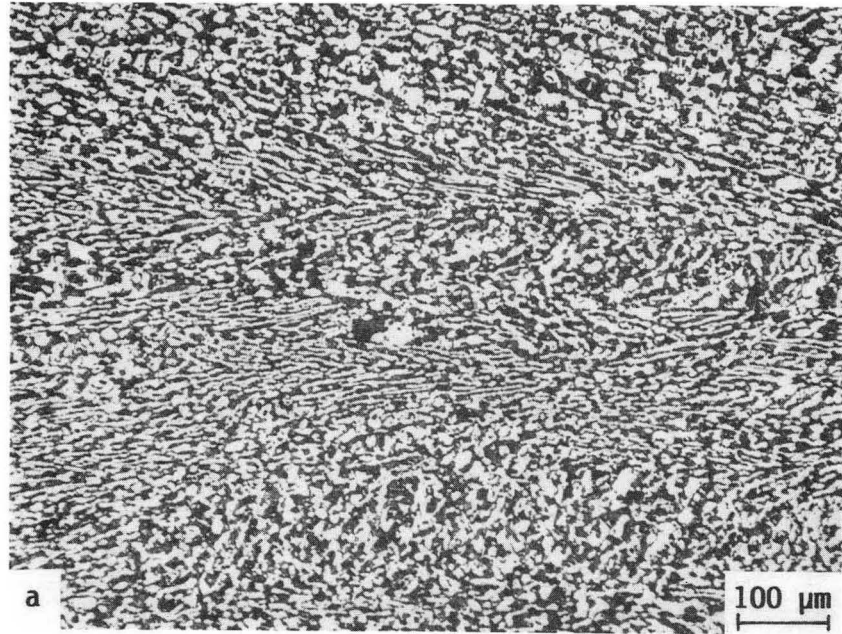


growth due to overload
large overload may change crack front shape-effectively reducing ΔK for subsequent growth

6) Pop-in

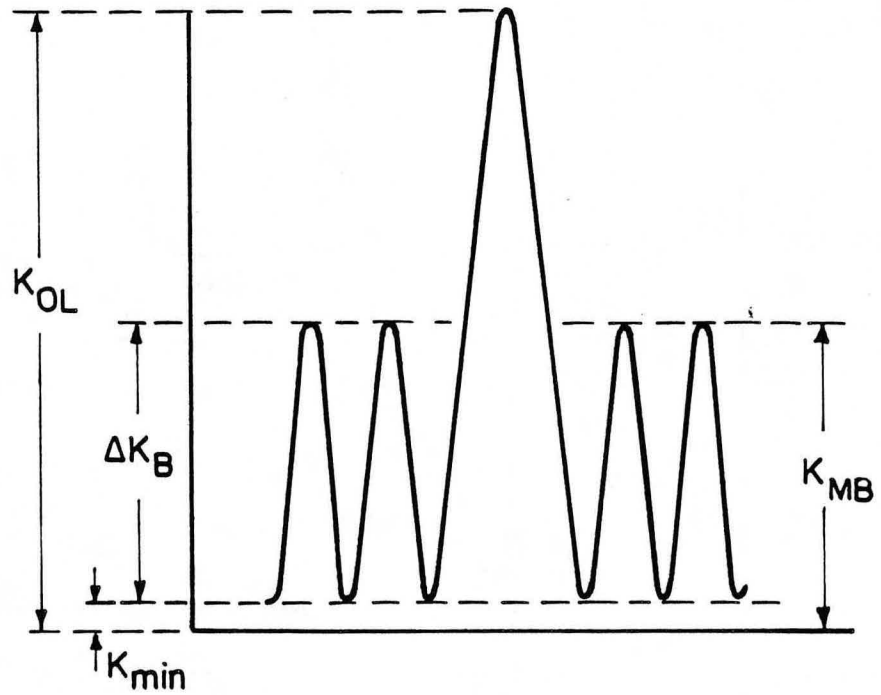
XBL 864-7618

Fig. 1. Schematic illustration of various proposed mechanisms to account for retardation following a tensile overload.



XBB 864-2938

Fig. 2. Optical micrographs of a) α/β -annealed (1 hr at 900°C, air cooled, 24 hr at 500°C), and b) β -annealed (1 hr 1010°C, air cooled, 24 hr at 500°C) microstructures.



K_{min} - minimum K

K_{MB} - maximum baseline K

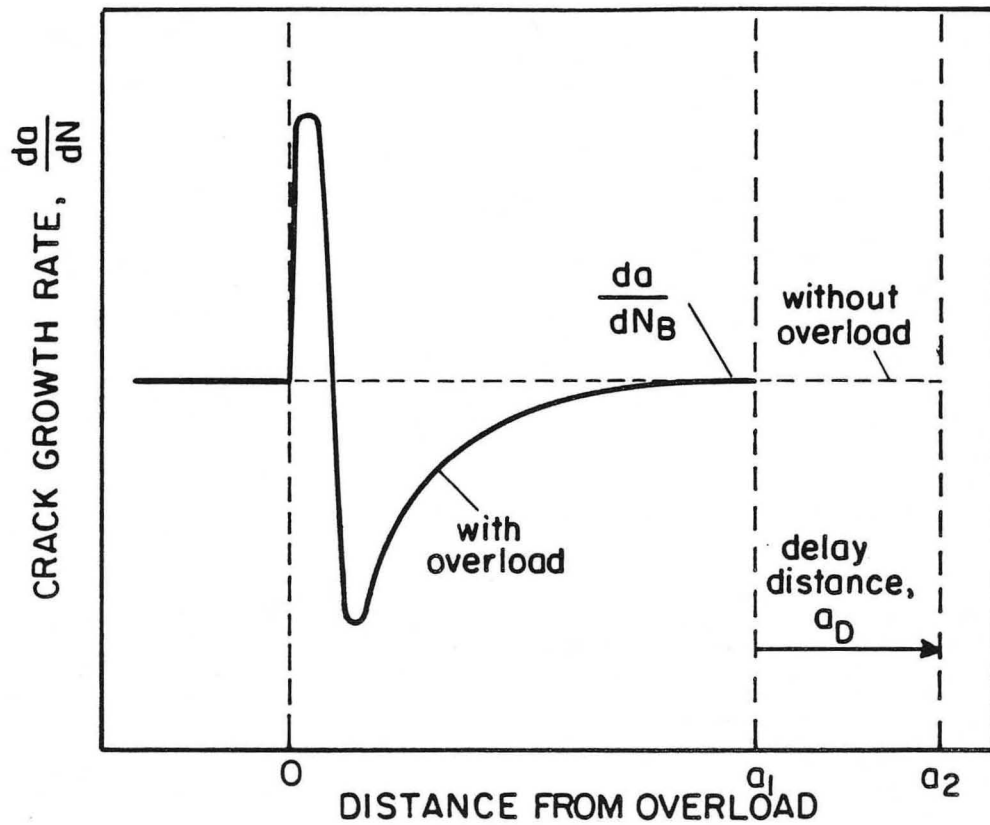
ΔK_B - baseline range of K

K_{OL} - maximum overload K

$$\text{overload magnitude} = \frac{K_{OL} - K_{MB}}{K_{MB}} \times 100\%$$

XBL864-7621

Fig. 3. Definition of parameters associated with single tensile overload.



$\frac{da}{dN_B}$ – baseline crack growth rate

a_1 – arbitrary distance from overload, beyond transient effects

N – cycles to reach a_1 (following overload)

a_2 – distance crack would have extended in N cycles (without an overload)

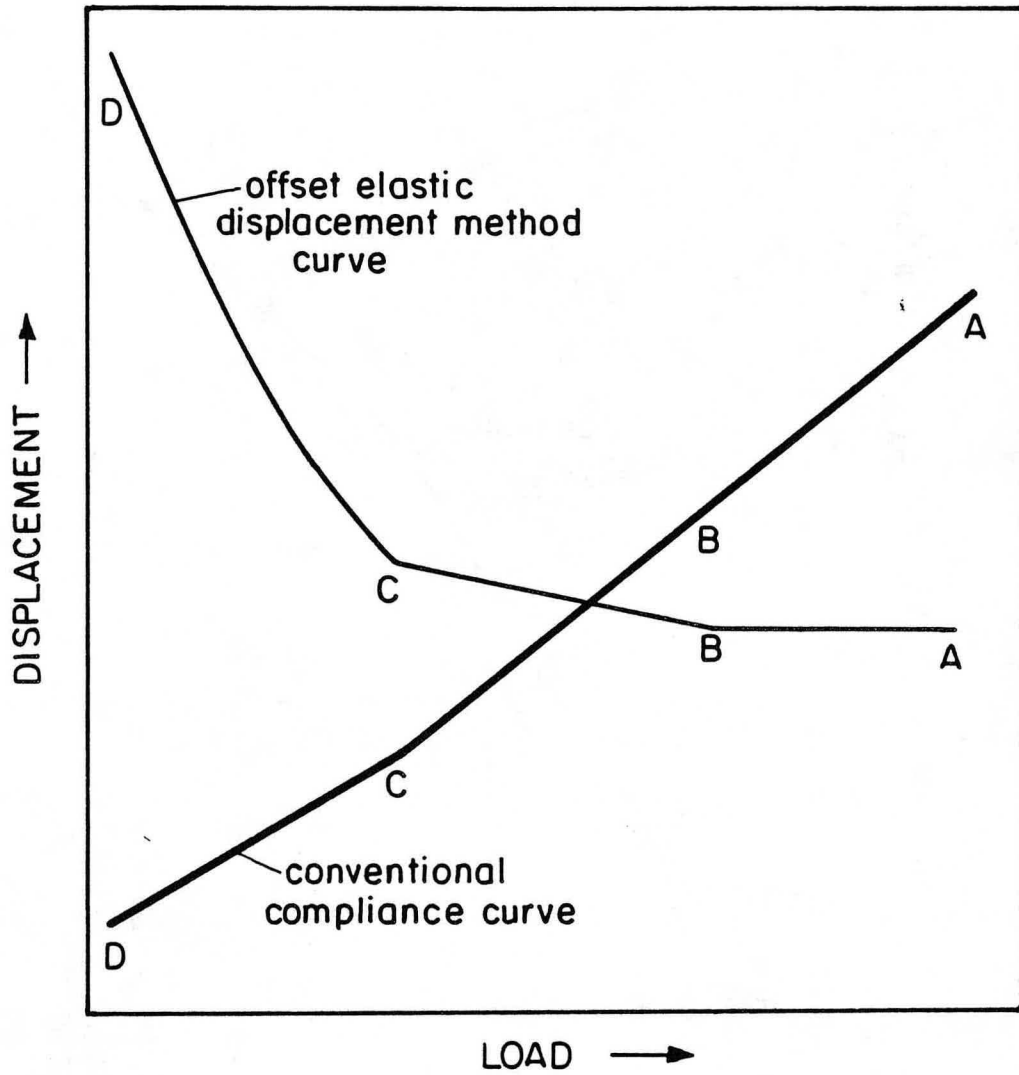
$$a_2 = N \times \frac{da}{dN_B}$$

$$\text{delay distance, } a_D = a_2 - a_1$$

$$\text{delay cycles, } N_D = a_D / \frac{da}{dN_B}$$

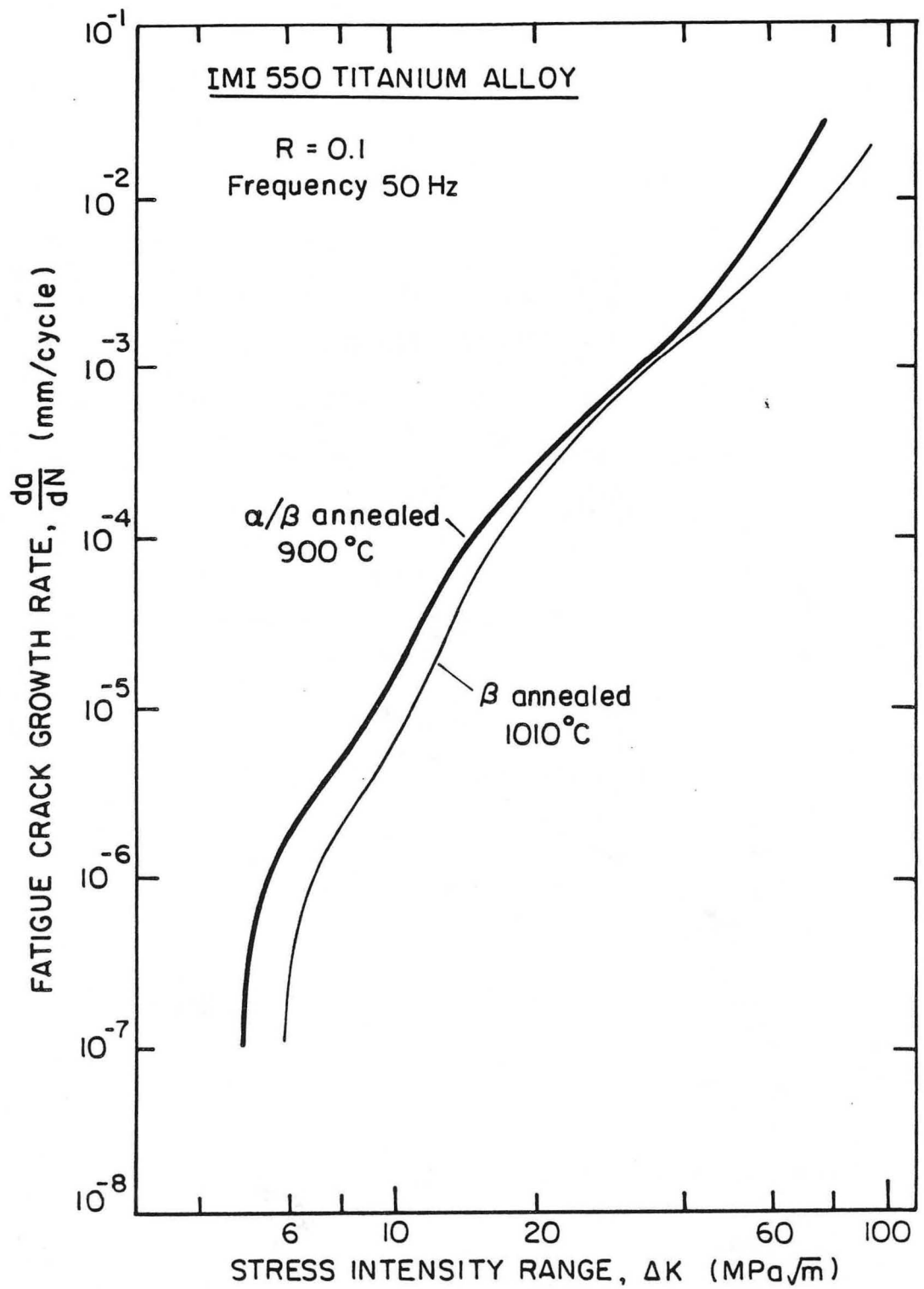
XBL 864-7619

Fig. 4. Schematic illustration of effect of a single tensile overload on crack growth at a constant baseline ΔK level, showing definition of delay distance and delay cycles.



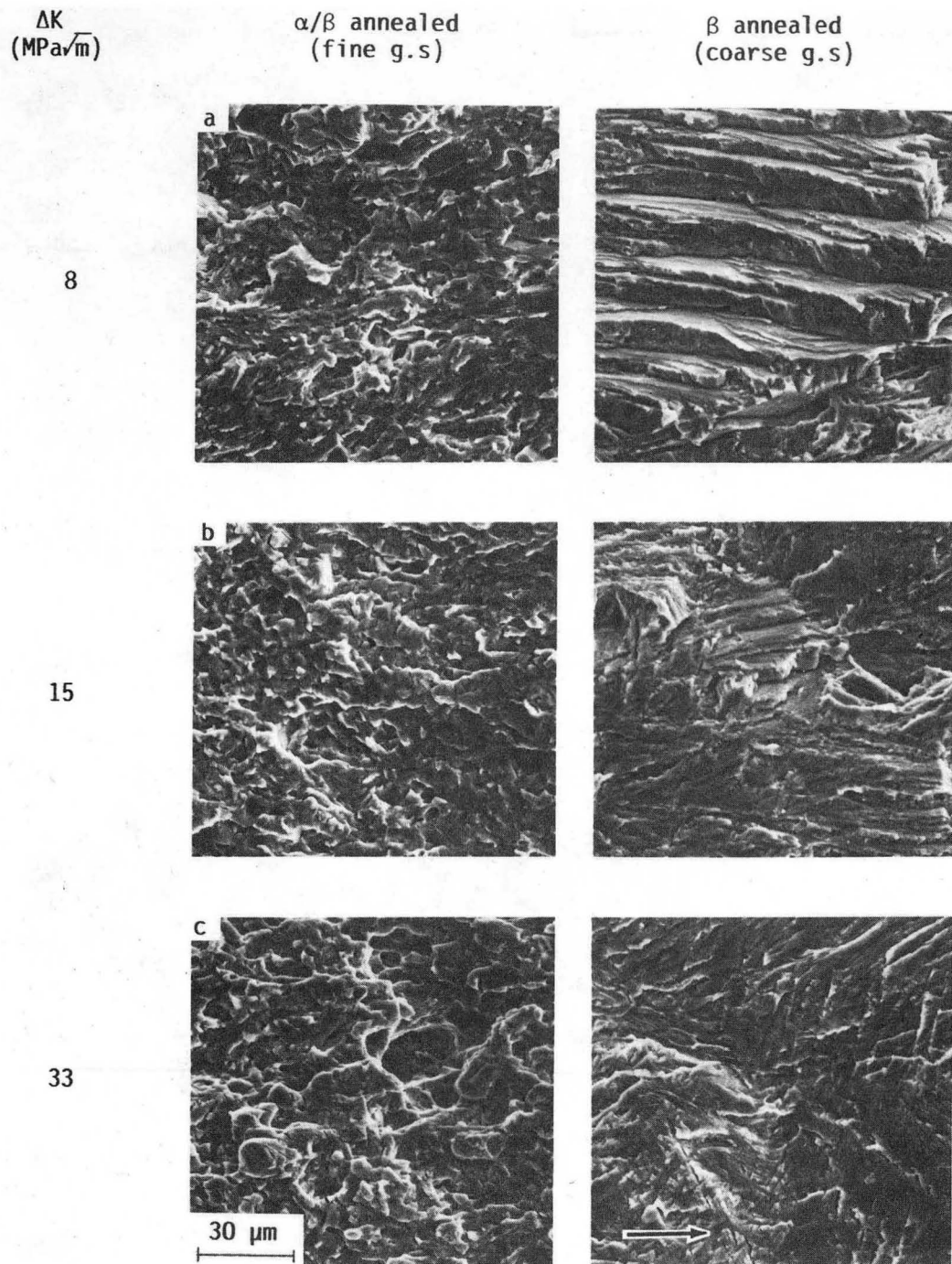
XBL 864-7622

Fig. 5. Illustration of conventional compliance curve, from back-face strain measurements, and its resultant offset elastic displacement curve, used to estimate closure stress intensities. Segment AB represents fully open crack, BC partial closure and CD final closure.



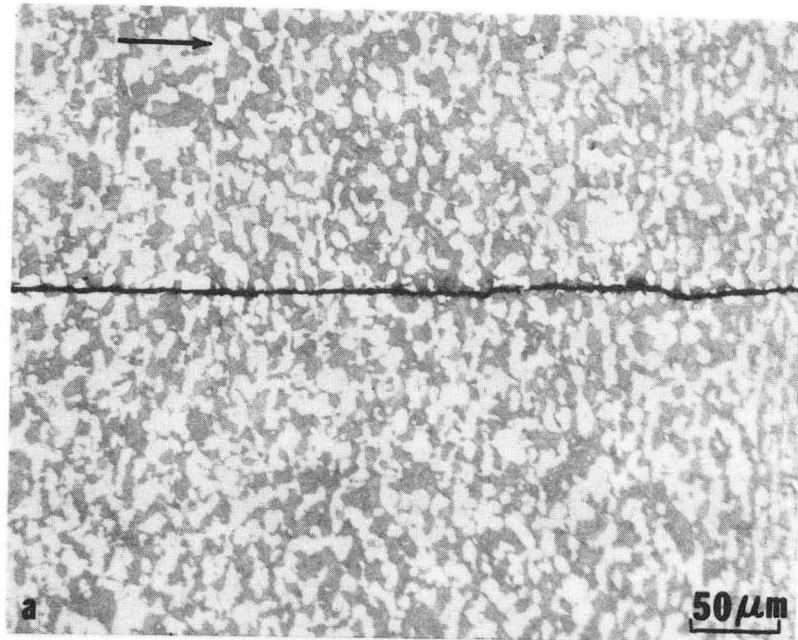
XBL 864-7620

Fig. 6. Constant amplitude fatigue crack propagation rates for IMI 550 titanium alloy at R = 0.1 with fine-grained α/β -annealed and coarse-grained β -annealed microstructures.



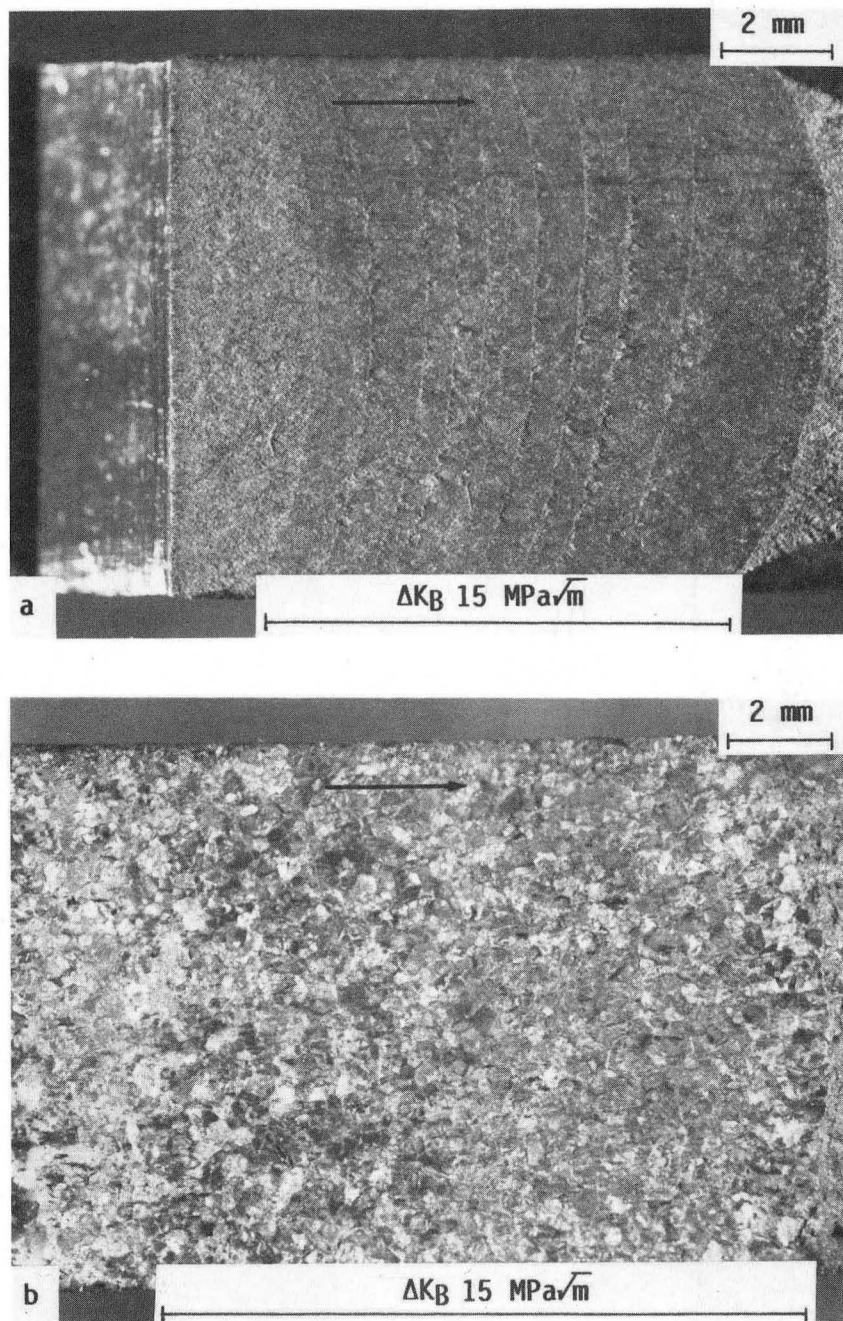
XBB 864-2940

Fig. 7. Scanning electron micrography of fatigue failure in fine-grained α/β -annealed and coarse-grained β -annealed microstructures of titanium alloy IMI 550 at a) $\Delta K = 8 \text{ MPa}\sqrt{\text{m}}$, b) $\Delta K = 15 \text{ MPa}\sqrt{\text{m}}$, and c) $\Delta K = 33 \text{ MPa}\sqrt{\text{m}}$ ($R = 0.1$).



XBB 864-2942

Fig. 8. Crack path morphology, at center section, of fatigue cracks in a) α/β -annealed and b) β -annealed microstructures at $\Delta K = 15 \text{ MPa}\sqrt{\text{m}}$ ($R = 0.1$).



XBB 864-2941

Fig. 9. Macroscopic views of the fatigue fracture surfaces of a) α/β -annealed and b) β -annealed microstructures, following 100% single tensile overload applied to a baseline ΔK of $15 \text{ MPa}\sqrt{\text{m}}$.

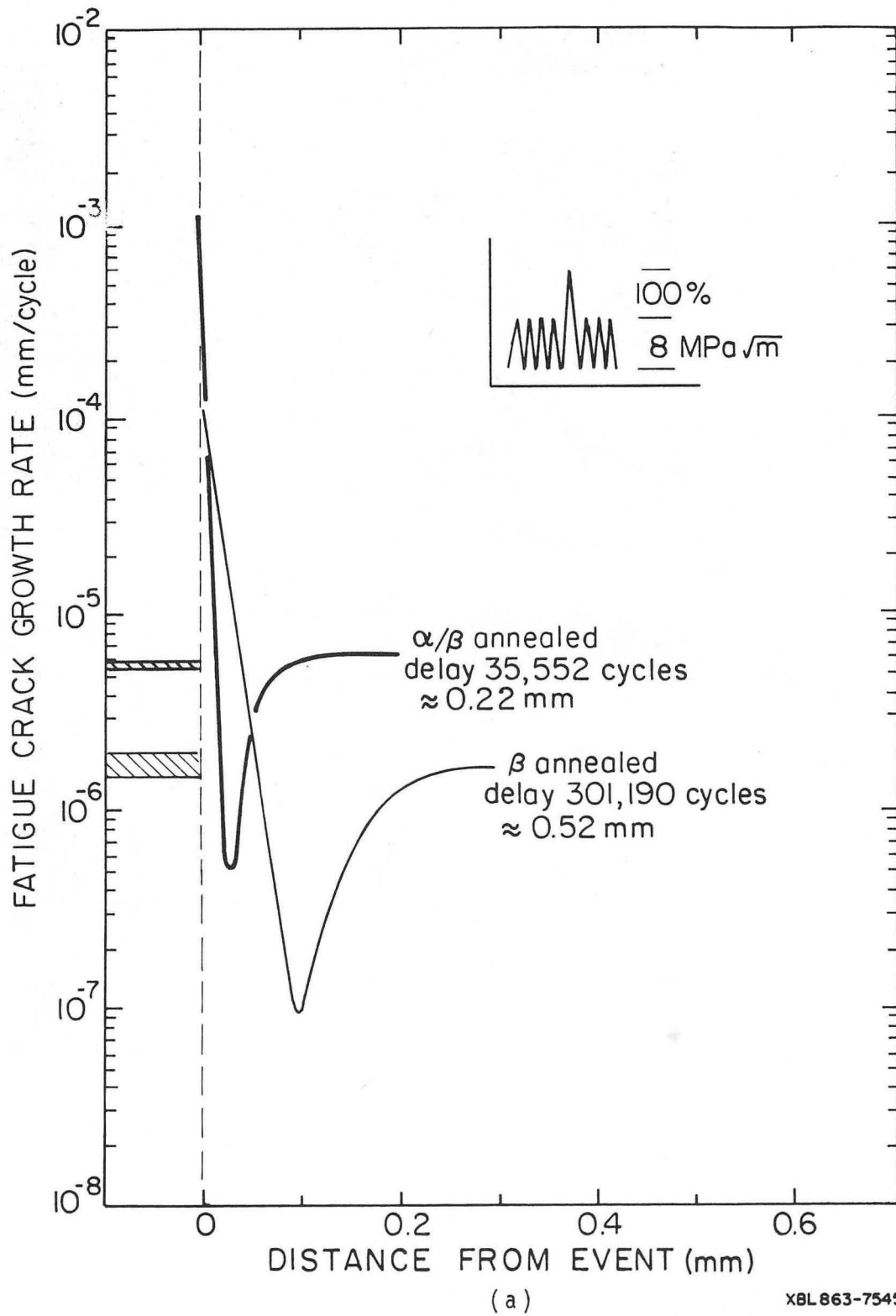
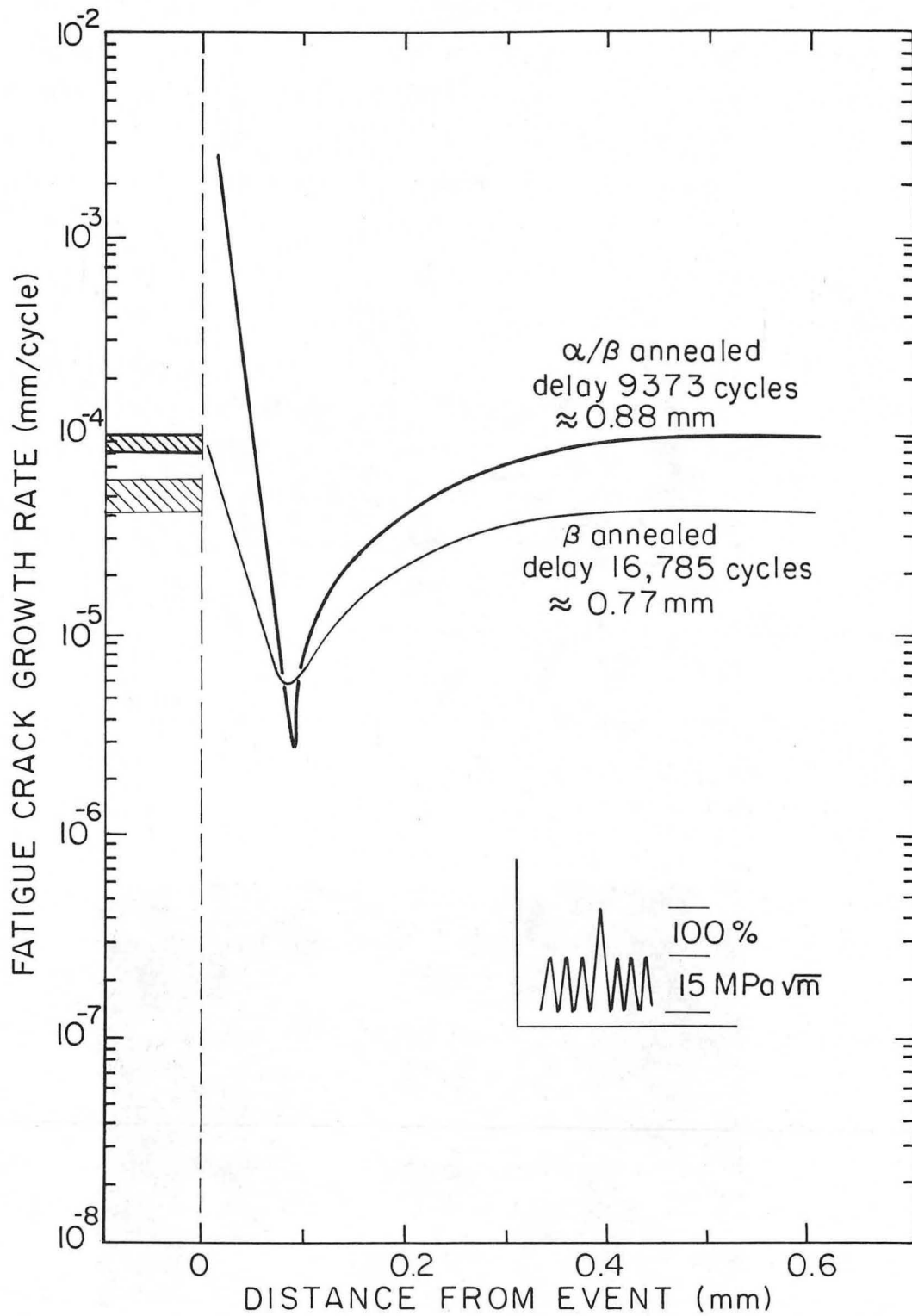
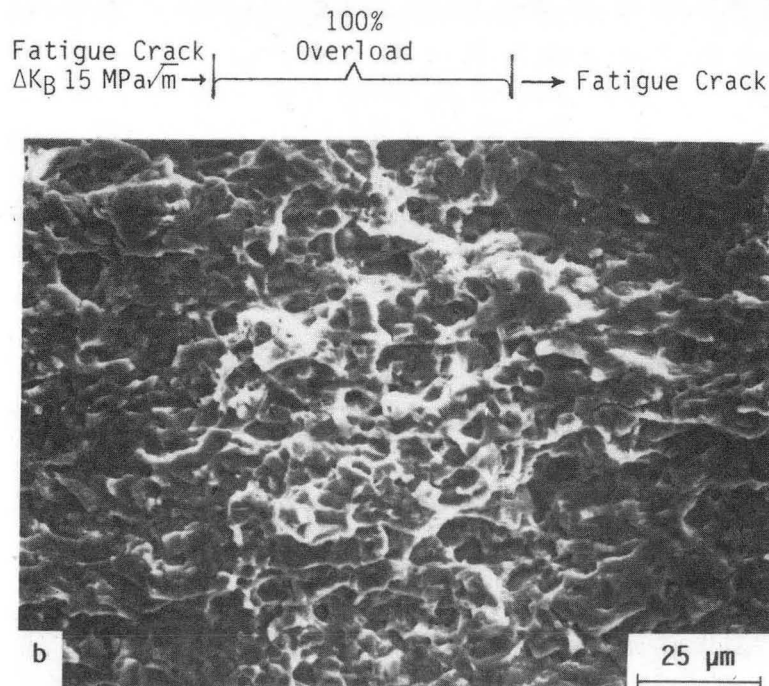
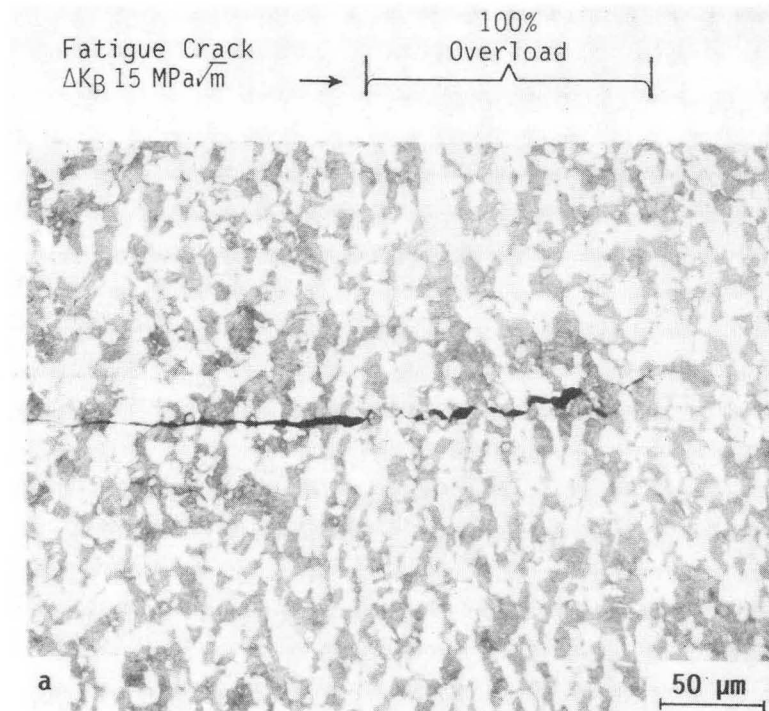


Fig. 10. Variation in fatigue crack growth rate in α/β -annealed and β -annealed microstructures following single 100% tensile overloads applied to baseline ΔK levels of a) $8 \text{ MPa}\sqrt{\text{m}}$ and b) $15 \text{ MPa}\sqrt{\text{m}}$.



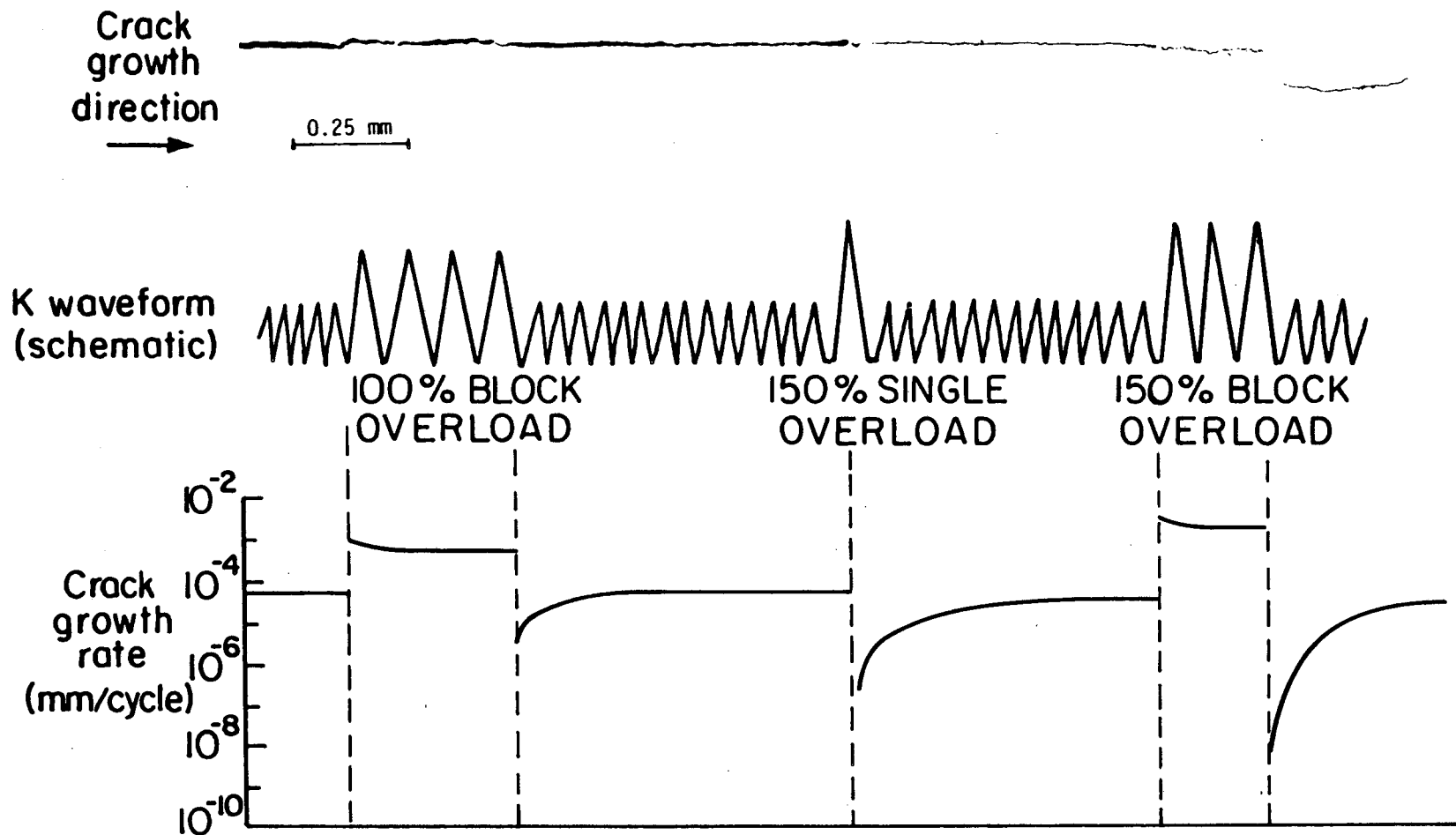
XBL863-7546

Fig. 10(b)



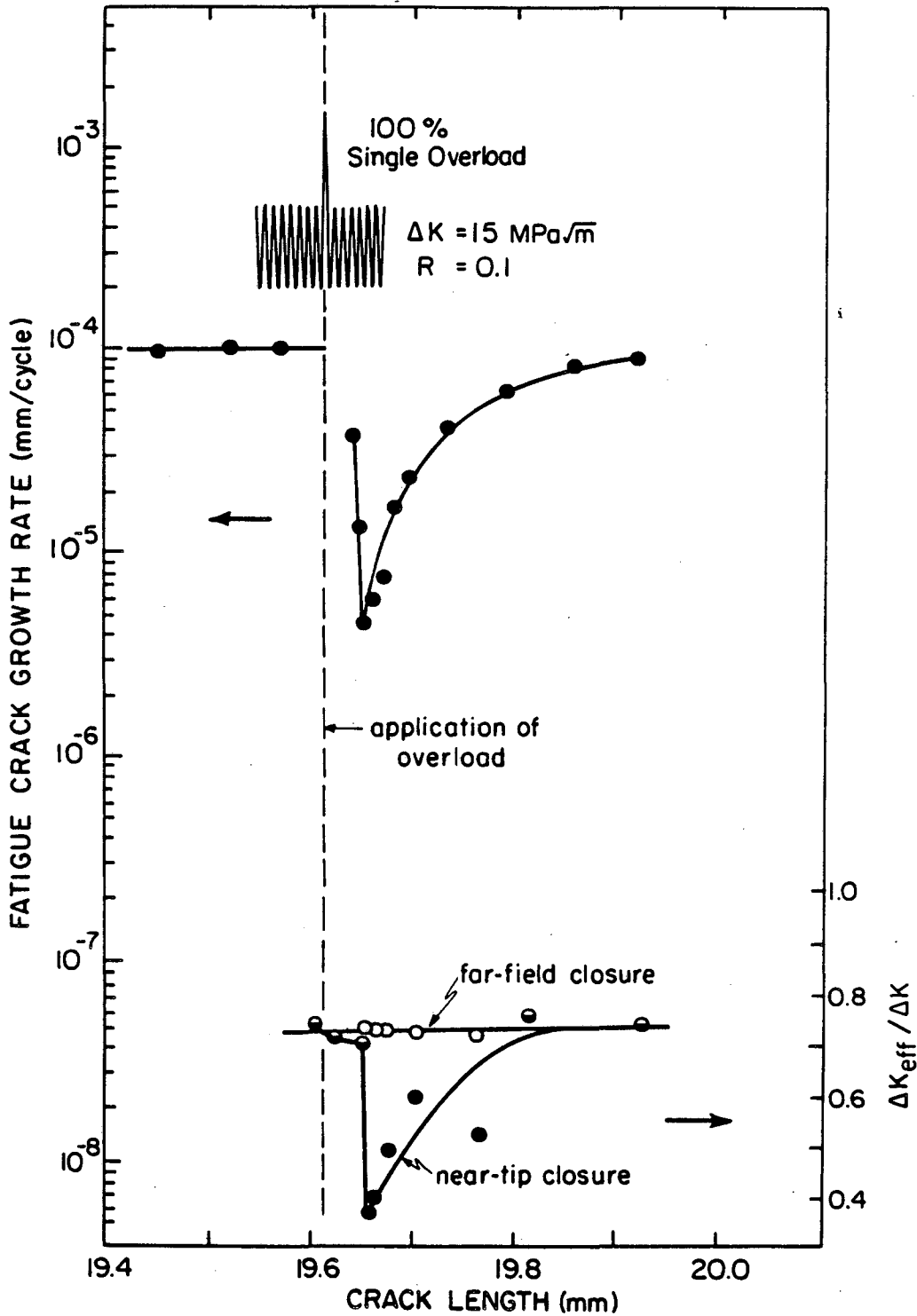
XBB 864-2939

Fig. 11. a) Optical micrograph of the crack path profile, at center section, in an α/β -annealed microstructure following 100% tensile overload at $\Delta K_B = 15 \text{ MPa}\sqrt{\text{m}}$. Note blunting at the pre-overload crack tip, and asperity contact is in region where crack extension occurred at the overload. b) Corresponding scanning electron micrograph of the fracture surface.



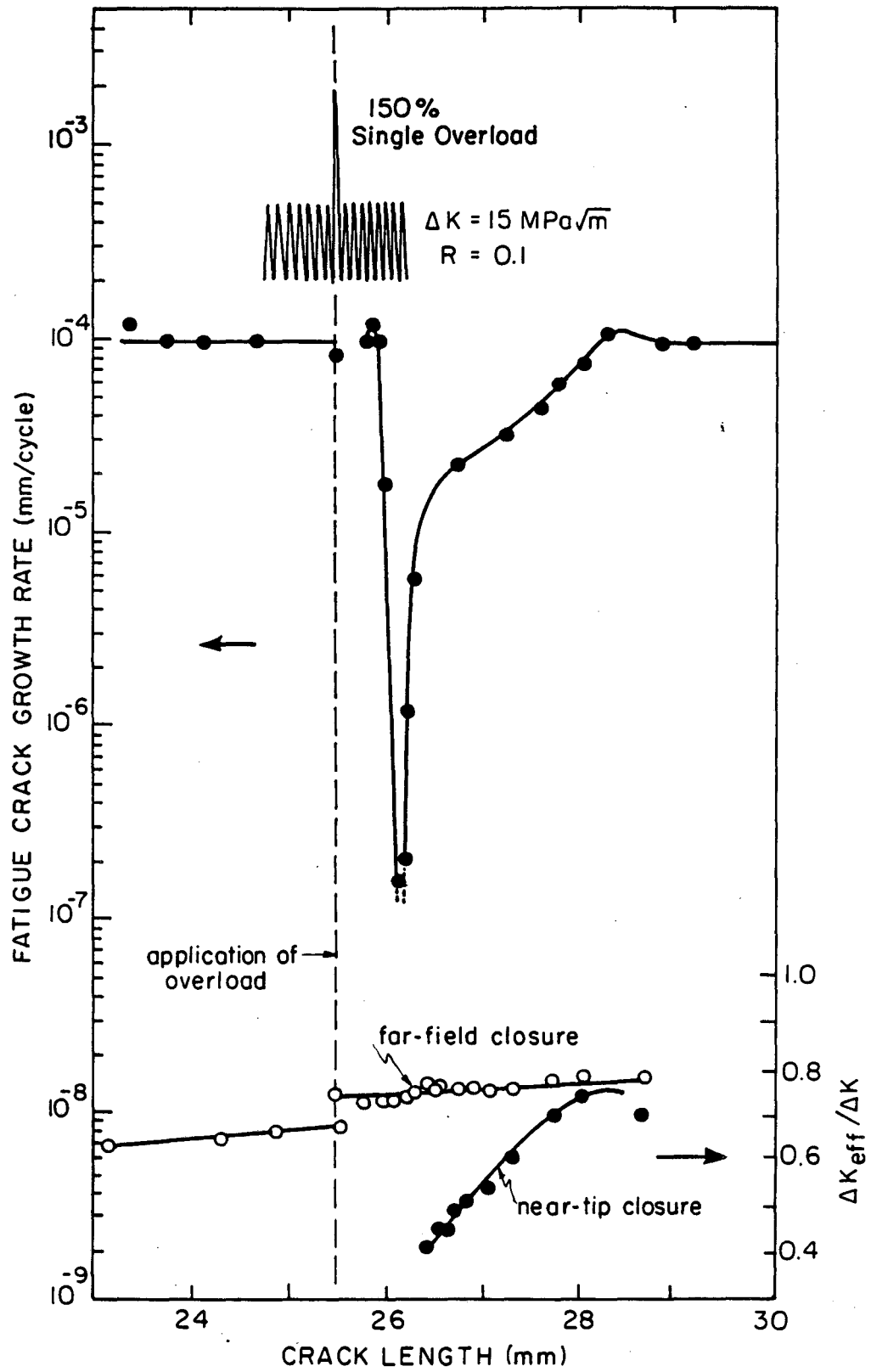
XBL863-7551

Fig. 12. Metallographic section through a fatigue crack in α/β -annealed microstructure subjected to 100% block overload, 150% single overload and 150% block overload at a constant baseline ΔK of $15 \text{ MPa}\sqrt{\text{m}}$, showing corresponding variation in growth rates. Note that after the single overload, crack blunting and opening occurs behind the tip, whereas the crack is closed directly ahead. Also significant crack deflection is only observed after the 150% high-low block loading sequence.



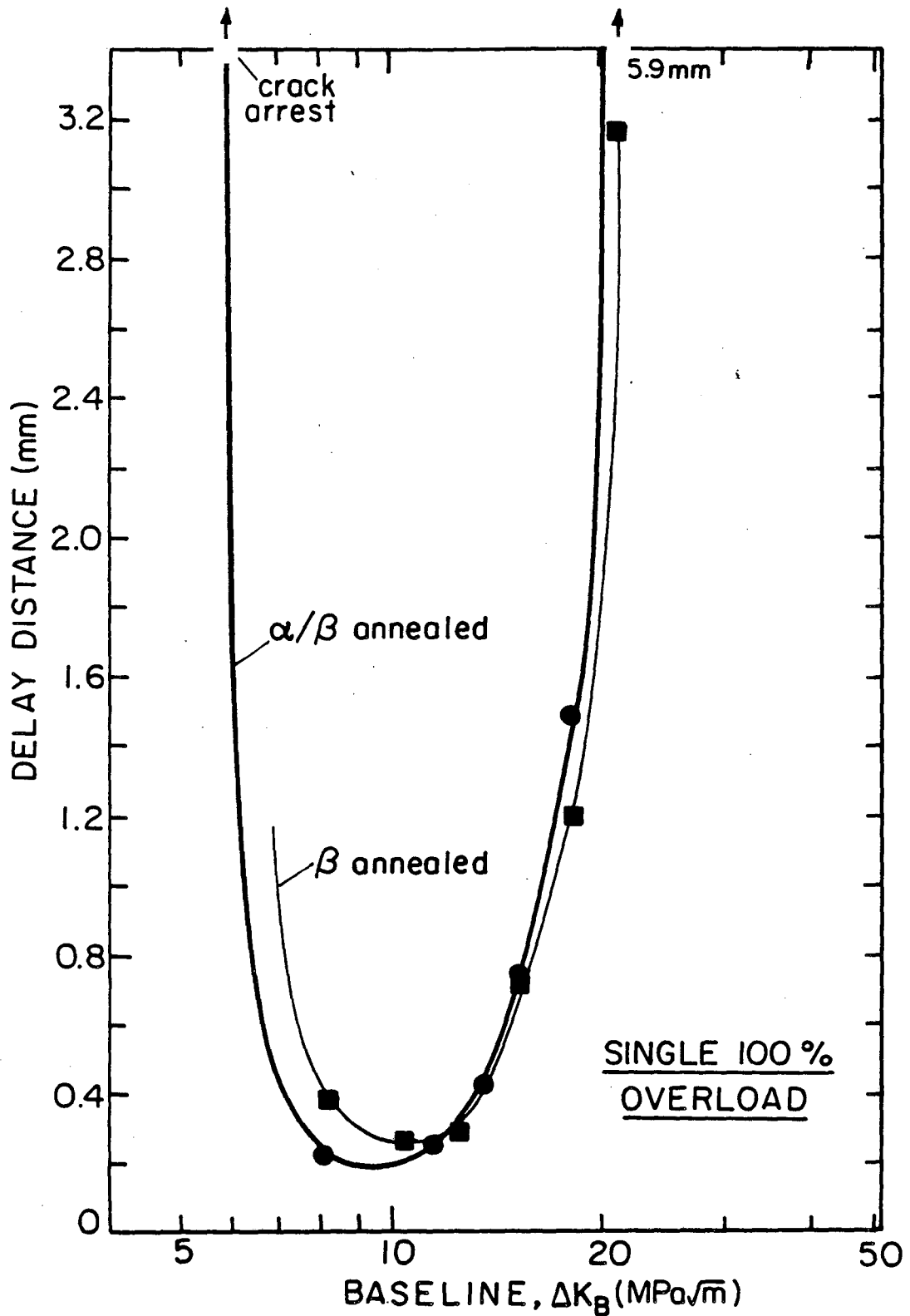
XBL 863-7552

Fig. 13. Variation in fatigue crack growth and corresponding variation in far-field and near-tip crack closure following a) 100% and b) 150% single tensile overloads at a constant baseline ΔK of $15 \text{ MPa}\sqrt{\text{m}}$ in α/β -annealed microstructure. Note how variation in local "driving force", ΔK_{eff} , corrected for near-tip closure, corresponds with the variation in post-overload growth rates.



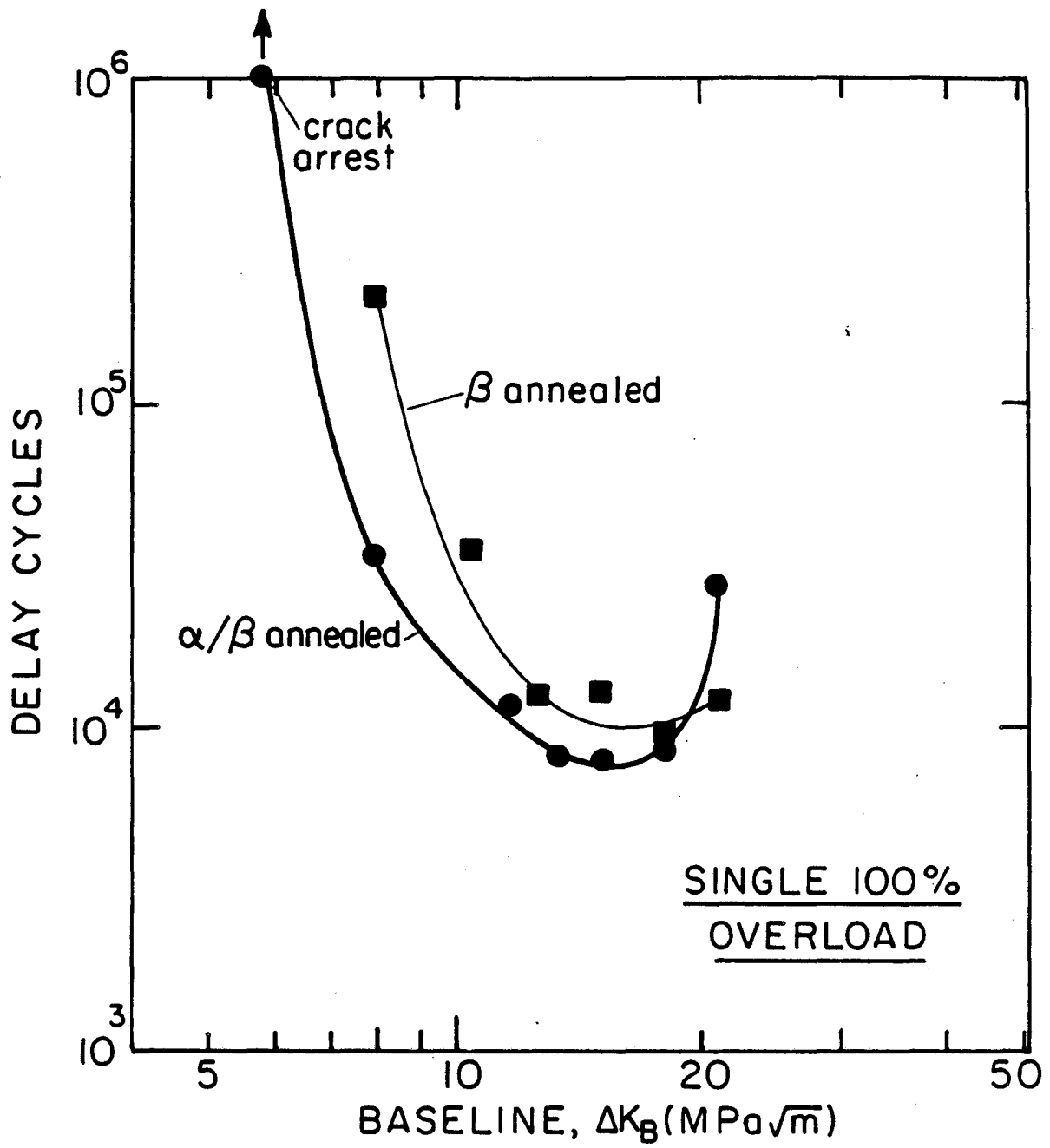
XBL 863-7553

Fig. 13(b)



XBL 863-7554

Fig. 14. Variation in post-overload retardation, measured in terms of a) delay distance and b) delay cycles, as a function of baseline ΔK level for 100% single tensile overloads in both α/β -annealed and β -annealed microstructures. Note how the delay is enhanced at either high or low stress intensity levels.



XBL 863-7556

Fig. 14(b)

*LAWRENCE BERKELEY LABORATORY
TECHNICAL INFORMATION DEPARTMENT
UNIVERSITY OF CALIFORNIA
BERKELEY, CALIFORNIA 94720*